International Journal of Multidisciplinary and Current Research ISSN: 2321-3124
Research Article Available at: http://ijmcr.com

Improvement of Mobility for In-Wheel Small Electric Vehicle with Integrated Four Wheel Drive and Independent Steering: A Numerical Simulation Analysis

Muhammad Izhar Ishak*, Hirohiko Ogino and Yoshio Yamamoto*****

*Graduate Student, Course of Science and Technology, Tokai University, Japan
**Department of Prime Mover Engineering, Tokai University, Japan
***Department of Precision Engineering, Tokai University, Japan

Accepted 10 April 2016, Available online 13 April 2016, **Vol.4 (March/April 2016 issue)**

Abstract

Similar to conventional vehicle, most in-wheel small electric vehicles (EV) that exist today are design with understeer (US) characteristic. We believe that oversteer (OS) design approach for in-wheel small EV can increase the steering response and lower the steering input. However, one disadvantage of OS characteristic is that it has a stability limit velocity. In this paper, we proposed a Four-Wheel Drive and Independent Steering (4WDIS) for in-wheel small EV with OS characteristic. The aim of implementing 4WDIS is to develop a high steer controllability and stability of an in-wheel small EV at any velocity. The 4WDIS is govern by an Intelligence Steering Control System (ISCS) that evaluates the dynamics of the EV, the surrounding condition, the road surface and vehicle stability in response to the drivers driving input. This paper analyses the steering performance of 4WDIS on an OS in-wheel small EV by using numerical simulation. The objective of the simulation is to model a control method for the 4WDIS by the ISCS based on the behavior of the OS in-wheel small EV before we can implement on an actual vehicle. The results show by implementing 4WDIS, an OS in-wheel small EV can achieve high cornering performance below the critical velocity while maintaining stability at high speed.

Keywords: *In-Wheel Small Electric Vehicle, Four Wheel Drive and Independent Steering, Oversteer Characteristic, Understeer Characteristic, Stability Limit Velocity, Numerical Simulation.*

1. Introduction

In recent years, concerns over environmental issues by petroleum-based transportations along with the issue of fossil fuel depletion around the world have led to renewed interest over electric vehicle (EV). Small EVs have become prominent as a mean of transportation, especially in urban areas where there are limited spaces [1, 2]. The driving method of an electric vehicle such can be divided into two types. The most basic type is the central motor system, where a conventional combustion engine is replaced with an electric motor. The other type is the in-wheel motor system, where a driving motor is located near the hub of each wheel. We believe that the in-wheel motor system has tremendous potential in the future of EVs for its compact size and high-energy efficiency. In past research, results show that the in-wheel motor system offers more freedom of movement for each wheel and can be governed separately by control systems such as the anti-lock brake system (ABS) and the traction control system (TCS) [3,4,5].

Car manufacturers such as Toyota and Honda have created a compact, cheap and reliable in-wheel small electric vehicle that aims for daily usage. Similar to conventional vehicle, most in-wheel small EVs that exist today are design with understeer (US) characteristic [6]. Even though they are safer on the road, they have poor cornering performance. With in-wheel motor and steer-by-wire technology, high cornering performance vehicle does not limit to only sport or racing cars. We believe that oversteer (OS) design approach for in-wheel small EV can increase the steering response and lower the steering input with shorter cornering radius. However, one disadvantage of OS characteristic is that it has a stability limit velocity [7]. In this paper, we proposed a Four-Wheel Drive and Independent Steering (4WDIS) for in-wheel small EV that is designed with OS characteristic. The aim of implementing 4WDIS is to develop a high steer controllability and stability of an OS in-wheel small EV at any velocity.

This paper analyses the performance of 4WDIS on an OS in-wheel small EV by using numerical simulation. Two cornering conditions were simulated which are 1) steady-state cornering at below critical velocity, and 2) steady state cornering over critical velocity. The objective of the simulation is to model a control method for the 4WDIS based on the behavior of the OS in-wheel small EV before we can implement on an actual vehicle. The 4WDIS is

govern by an Intelligence Steering Control System (ISCS) that evaluates the dynamics of the EV, the surrounding condition (i.e. narrow space), the road surface (i.e. dry, wet and icy road) and vehicle stability (i.e. crosswind and soft collision) in response to the drivers driving input. The ISCS will control the four wheel driving and braking with each in-wheel motors, and steer angle by the steering actuators to ensure safe maneuverability. The results show by implementing 4WDIS, an OS in-wheel small EV can achieve high cornering performance and maintain stability at any speed.

2. Main Symbols

b: width of tire interacted surface = 0.1 m , d_F: front tread = 0.84 m , d_R: rear tread = 1.280 m, H: high gain in feedback control system = 20, I: yaw inertia moment at gravity point of vehicle = 1470 kgm^2 , K_x, K_y : front and rear wheel stiffness = 3.33x10^6 N/m^3 , K_F, : front wheel cornering power = 2000 N/rad , K_R : rear wheel cornering power = 2612.62 N/rad, l: length of tire interacted surface = 0.15 m , l_F: length from front axle to gravity point of vehicle = 0.64 m , l_R: length from rear axle to gravity point of vehicle = 0.64 m , m: mass of the vehicle = 421.61 kg , u: longitude velocity, v: lateral velocity, V: velocity at center gravity, Vc: Stability limit velocity, X_{FR},X_{FL},X_{RR},X_{RL},: friction force for each tire, Y_{FR},Y_{FL},Y_{RR},Y_{RL},: lateral force for each tire, W_z: wheels load subject to load transfer, β: side slip angle of vehicle, β^*: side slip angle of state observer, β_{FR}, β_{FL}, β_{RR}, β_{RL}: tire side slip angle, μ: friction coefficient, ϑ_F, ϑ_R :front and rear tire steer angle, γ: yaw rotational speed of vehicle body, γ^*: yaw rotational speed of state observer, ρ: slip ratio, ω : wheel rotational speed.

3. Limitation of OS and US Characteristics

A basic understanding of OS and US characteristic is necessary before any control method can be implemented. Fig.1 shows the relationship of the steady state yaw rotational speed to velocity, and fig.2 show the relationship of steady state side slip angle to velocity between OS and US characteristic during steady state cornering at constant steer angle. Based on the figure, the OS characteristic is separated into stable region and unstable region depending on the velocity of the vehicle. When the vehicle velocity V is below the stability limit velocity Vc, OS vehicle can achieve steady state cornering with a higher yaw rotational speed in comparison to US characteristic. A higher yaw rotational speed should also means that the vehicle can achieve a shorter turning radius. The side-slip angle becomes negative as the absolute magnitude increases with velocity. This means that when the velocity increases, the vehicle will point into the inner side of the circular path of the cornering.
However, in the case of the velocity $V \geq Vc$, the yaw rotational speed and the side-slip angle will produce an infinite value in regards to a constant steer angle. It does not mean that the vehicle cannot be driven above this velocity but it is important to note that the vehicle motion is unstable. For this particular reason, most vehicles are manufactured with US characteristic that has no stability limit velocity as a compensation to low steering response.

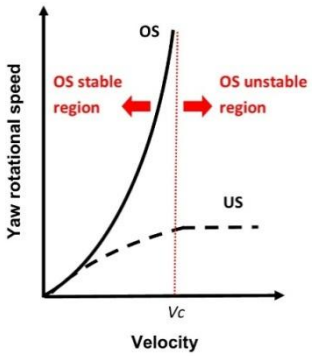

Fig.1 Steady state yaw rotational speed to velocity between OS and US characteristic

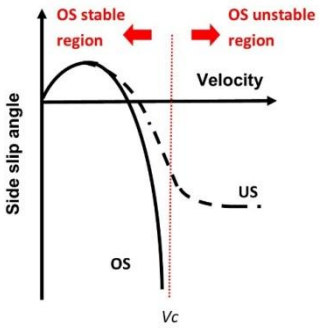

Fig.2 Steady stateside-slip angle to velocity between OS and US characteristic

Nonetheless, US vehicle also has a tendency to cause accidents at high speed due to its restrictive steering.

4. Four Wheel Drive and Independent Steering (4WDIS) Approach

4.1 Steering characteristics

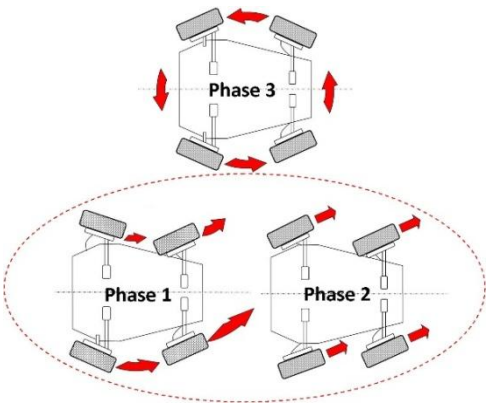

Fig.3 4WDIS steering characteristics

The main purpose of implementing 4WDIS is to have high cornering performance for OS in-wheel small EV while maintain stability at any speed. In-wheel motor system and steer by-wire technology allows a small electric vehicle the freedom of movements and layouts [8]. Considering that each wheels' driving torque can be governed separately and the direction of the wheels can be manipulated with certain control, we had concluded that the steering modes for 4WDIS can be separated as follow;

a) Opposite steering (Phase 1)
The rear wheels will turn on the opposite direction as the front wheels. This will increase the vehicle yaw rotational speed, which tighten the turning radius.
b) Parallel steering (Phase 2)
The rear wheels will rotate in the same direction parallel to the front. This steering does not generate yaw rotational speed.
c) 'Zero-radius' steering (Phase 3)
The front wheels have to be 'toe-in' position and the rear wheels in 'toe-out' position. The driving direction of the left and right is in opposite. This allows the vehicle to rotate at its yaw rotational center.

4.2 Intelligence Steering Control System (ISCS)

An Intelligence Steering Control System (ISCS) is used to govern the 4WDIS. The ISCS evaluates the dynamics of the EV, the surrounding condition (i.e. narrow space), the road surface (i.e. dry, wet and icy road) and vehicle stability (i.e. crosswind and soft collision) with regard to the drivers steering input. After the evaluation, the ISCS will choose the suitable steering characteristics to ensure stability and maneuverability.

In this paper, the evaluated parameter is focus on the dynamic of the in-wheel small EV and dry road surface. Thus, when studying the cornering performance of OS in-wheel small EV, only the alternation between phase 1 and 2 as show in fig.3 can be observed in the results.

5. Analysis Vehicle Model

Fig.4 Analysis vehicle model of Toyota COMS

Table 1 Specifications of Toyota COMS

Vehicle actual mass	361.9 (kg)
Maximum Speed	50 (km/h)
Height of center gravity	0.105 (m)
Tread front	0.840 (m)
Tread rear	1.280 (m)
Wheel base	0.430 (kgm^2)
Driving system	2 in-wheel motor
Steering system	Front wheel steering
Maximum front steer angle	20 (^{o})

Toyota COMS AK10E-PC shown in fig.4, which is an in-wheel small electric vehicle manufactured by Toyota Auto Body Co, was used as an analysis vehicle model in the simulation. The specifications of the actual vehicle are provided in Table 1. It is stated that the vehicle uses a 2WD in-wheel motor and has a front-wheel steering. However, in the simulation, we added two in-wheel motors to the front wheels and two steering actuator at the rear wheels. Thus, the mass of the vehicle model is increased from the actual vehicle. Furthermore, the weight distribution of the vehicle model was modified so that the weight shifted to the rear to represent as a highly OS in-wheel small EV while the dimensions of the vehicle remain the same.

6. Simulation Block Diagram

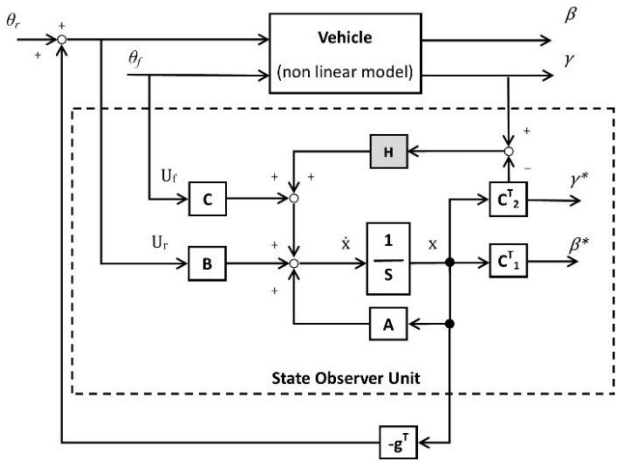

Fig.5 Simulation block diagram

Figure 5 shows the simulation block diagram for the vehicle model and the ISCS. The vehicle model, which is an OS in-wheel small EV equipped with 4WDIS, is calculated by a nonlinear system. Much of past researches adopted easy way of modelling a control system based on a vehicle with linear characteristics. By this assumption, other parameters that could influenced the dynamic motion of the vehicle are neglected and the modelled control system deem low precision [9, 10, 11, 12]. In this paper, the purpose of adopting nonlinear system for calculating the vehicle model is that the system represent more precisely of an actual vehicle.

However, a feedback control cannot be executed directly to nonlinear system because of yaw rotational speed coupling with the velocity components as expressed in dynamic equation of motion in later section. As an option, the ISCS, which is a state observer unit that consist of a feedback controlled linear system, is used to control the vehicle model. Each model in the simulation block will be explain in detail in the following sections.

7. Vehicle model Nonlinear Dynamic Equations

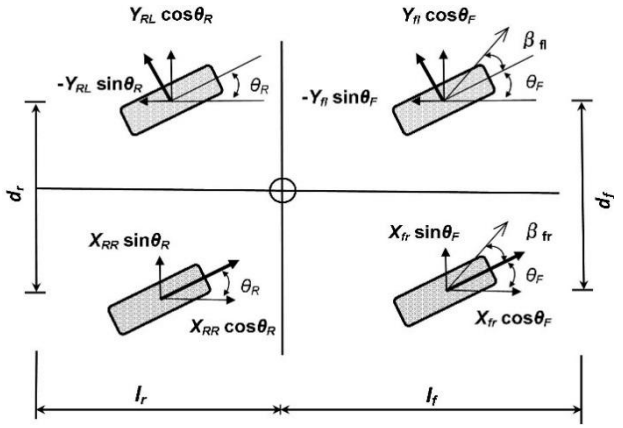

Fig.6 Force vector

The vehicle model has six degrees of freedom: three translational along the *x, y,* and *z*-axes, and three rotational about the *x, y* and *z*-axes. In this study, however, a planar motion is assumed so that a translation along the z-axis and rotations about the x and y-axes are disregarded. Fig.6 depicts the force vector used to construct the dynamic equations of motion for the vehicle and for the yaw rotational speed.

The assumption made necessitates us to calculate the dynamic equations for longitude and latitude velocities, including the coupling of the yaw rotation speed with the velocities.

$$\begin{aligned} \mathrm{m}\left(\frac{du}{dt}-v\gamma\right) &= (X_{FR}+X_{FL})\cos\theta_F \\ &+(X_{RR}+X_{RL})\cos\theta_R \\ &-(Y_{FR}+Y_{FL})\sin\theta_F \\ &-(Y_{RR}+Y_{RL})\sin\theta_R \end{aligned} \quad (1)$$

$$\begin{aligned} \mathrm{m}\left(\frac{dv}{dt}+u\gamma\right) &= (X_{FR}+X_{FL})\sin\theta_F \\ &+(X_{RR}+X_{RL})\sin\theta_R \\ &+(Y_{FR}+Y_{FL})\cos\theta_F \\ &+(Y_{RR}+Y_{RL})\cos\theta_R \end{aligned} \quad (2)$$

$$\begin{aligned} \mathrm{I}\frac{d\gamma}{dt} &= l_F[(X_{FR}+X_{FL})\sin\theta_F+(Y_{FR}+Y_{FL})\cos\theta_F] \\ &+l_R[(X_{RR}+X_{RL})\sin\theta_R+(Y_{RR}+Y_{RL})\cos\theta_R] \\ &+\frac{d_F}{2}[(X_{FR}+X_{FL})\cos\theta_F+(Y_{FR}+Y_{FL})\sin\theta_F] \\ &+\frac{d_R}{2}[(X_{RR}+X_{RL})\cos\theta_R+(Y_{RR}+Y_{RL})\sin\theta_R] \end{aligned} \quad (3)$$

Each wheels of the vehicle are modelled as a brush tire. Due to this, the equations for friction and lateral forces are dependent on the value of slip ratio, tire side-slip angle, and weight distribution. The model's deformation of the tire tread rubber is also used to derive the following equations,

$$\xi_p = 1-\frac{K_\rho\lambda}{3\mu W_z(1-\rho)}$$

$$\lambda = \sqrt{\rho^2+\left(\frac{K_\beta}{K_\rho}\right)^2\tan^2\beta}$$

$$K_\rho = \frac{b{l_T}^2}{2}K_x \quad , \quad K_\beta = \frac{b{l_T}^2}{2}K_y$$

If $\xi_\rho \geq 0$

$$X = -K_\rho\rho{\xi_p}^2 - 6\mu W_z\frac{\rho}{\lambda}\left(\frac{1}{6}-\frac{1}{2}{\xi_p}^2+\frac{1}{3}{\xi_p}^3\right)$$

$$\begin{aligned} Y &= -K_\beta(1+\rho)\tan\beta\,{\xi_p}^2 \\ &-6\mu W_z\left(\frac{K_\beta\tan\beta(1+\rho)}{K_\rho\lambda}\right)\left(\frac{1}{6}-\frac{1}{2}{\xi_p}^2+\frac{1}{3}{\xi_p}^3\right) \end{aligned} \quad (4)$$

Else

$$X = -\mu W_z\frac{\rho}{\lambda}$$

$$Y = -\mu W_z\left(\frac{K_\beta\tan\beta(1+\rho)}{K_\rho\lambda}\right) \quad (5)$$

The equation for side-slip angle for each tire is given as follows,

$$\begin{aligned} \beta_{FR} &= \tan^{-1}\left(\frac{v+l_F\gamma}{u+d_F\gamma/2}\right)-\theta_F \\ \beta_{FL} &= \tan^{-1}\left(\frac{v+l_F\gamma}{u-d_F\gamma/2}\right)-\theta_F \\ \beta_{RR} &= \tan^{-1}\left(\frac{v-l_R\gamma}{u+d_R\gamma/2}\right)-\theta_R \\ \beta_{RL} &= \tan^{-1}\left(\frac{v-l_R\gamma}{u-d_R\gamma/2}\right)-\theta_R \end{aligned} \quad (6)$$

The slip ratio ρ can be represented in terms of the traction between the road and the tire surface, which is defined as

$$\rho = \frac{r\omega-u}{r\omega} \quad (7)$$

Then the coefficient of friction μ can be approximated by the following equation

$$\mu = -1.10\mathrm{k} \times (e^{35\rho} - e^{0.35\rho}) \quad (8)$$

Where

$$\begin{cases} k = 1.0 \ \ (dry\ asphalt) \\ k = 0.2 \ \ (icy\ road) \end{cases}$$

8. State Observer Unit

8.1 Linear Dynamic Equation

The ISCS consist of a state observer unit. This unit uses linear dynamic equations for the translational motion and yaw rotational motion such as,

$$\mathrm{m}v\left(\frac{d\beta^*}{dt} + \gamma^*\right) = 2Y_f + 2Y_r \quad (9)$$

$$\mathrm{I}\frac{d\gamma^*}{dt} = (2l_f Y_f - 2l_r Y_r)\cos\beta^* \quad (10)$$

It is to be noted that there is no difference in the characteristics of the left and right tires due to linearity; hence, a 2-wheel model is derived from the equations. If the side-slip angle is small, it is assumed that the direction perpendicular to the traveling direction of the vehicle almost coincides with the lateral direction *y*. Therefore, no coupling exists between the yaw rotational speed and the vehicle's translational velocity.

The linear lateral force is defined by

$$Y_f = -K_f\beta_f = -K_f\left(\beta^* + \frac{l_f}{v}\gamma^* - \theta_f\right) \quad (11),$$

$$Y_r = -K_r\beta_r = -K_r\left(\beta^* - \frac{l_r}{v}\gamma^* - \theta_r\right) \quad (12)$$

Here, the cornering power of the front and rear wheels, K_F and K_R, are chosen by the designer. These values determine the sensitivity of the ISCS. In contrast, with the tire characteristics of the nonlinear model, the actual vehicle motion determines the linear model lateral forces, which are related to the side-slip angle, yaw rotational speed, and front and rear steering angles. The above equations can be substituted into the linear dynamic equations of motion eq. (9) and the yaw rotational speed eq. (10).

8.2 Linearized Differential Equation

The linearized differential equation represents the linear vehicle dynamic equation of motion for the state observer. It is arranged as a set of first-order ordinary differential equations in the vector state form:

$$\dot{\mathrm{x}} = \mathrm{Ax} + \mathrm{BU}_r + \mathrm{CU}_f$$

$$y_\beta = \beta^* = {\mathbb{C}_1}^T\mathrm{x}$$

$$y_\gamma = \gamma^* = {\mathbb{C}_2}^T\mathrm{x} \quad (13)$$

Where,

$$\mathrm{x} = [\beta^* \quad \gamma^*]^T,$$
$${\mathbb{C}_1}^T = [1 \quad 0]^T, \qquad \mathrm{U}_f = \theta_F,$$
$${\mathbb{C}_2}^T = [0 \quad 1]^T, \qquad \mathrm{U}_r = \theta_R,$$

$$\mathrm{A} = \begin{bmatrix} a & b \\ c & d \end{bmatrix} = \begin{bmatrix} -\frac{2(K_f + K_r)}{mv} & -1 - \frac{2(K_f l_f - K_r l_r)}{mv^2} \\ -\frac{2(l_f K_f - l_r K_r)}{I} & \frac{2({l_f}^2 K_f + {l_r}^2 K_r)}{Iv} \end{bmatrix}$$

$$\mathrm{B} = \begin{bmatrix} e \\ f \end{bmatrix} = \begin{bmatrix} \frac{2K_r}{mv} \\ -\frac{2l_r K_r}{I} \end{bmatrix}$$

$$\mathrm{C} = \begin{bmatrix} k \\ l \end{bmatrix} = \begin{bmatrix} \frac{2K_f}{mv} \\ \frac{2l_f K_f}{I} \end{bmatrix}$$

The state vector x represents the side-slip angle and yaw rotational speed of the vehicle. The steering angles of the front and rear wheels are the inputs of this system. The value for the front-wheel angle ϑ_F is a driver-selected input whereas the rear-wheel angle ϑ_R is initially 0 degrees. During high-speed cornering, the rear-wheel steering is used as the control input by introducing a feedback gain $-g^T$.

$$\mathrm{U}_r = -g^T\mathrm{x} + \theta_r \quad (14)$$

8.3 Optimal Control

In order to find the optimal control for the linearized differential equation, the following evaluation function *J* is employed.

$$J = \int_0^\infty (q_{11}\mathrm{x}^2 + q_{22}\dot{\mathrm{x}}^2 + w\theta_r^2)dt$$
$$= \int_0^\infty (\mathrm{x}^T Q\mathrm{x} + w\theta_r^2)dt \quad (15)$$

Where,

$$\mathrm{Q} = \begin{bmatrix} q_{11} & 0 \\ 0 & q_{22} \end{bmatrix}$$

in which q_{11}, q_{22}, and *w* are appropriately chosen constant weighting matrices for the side-slip angle, yaw rotational speed, and rear-wheel steering angle, respectively. The optimal solution for *J* can be designed if Q is a positive definite matrix and the state observer control input U_r is given b

$$\mathrm{U}_r = -\frac{1}{w}B^T P\mathrm{x} + \theta_R \quad (16)$$

Where,

$$-\mathrm{g}^T = -\frac{1}{w}B^T P$$

With P = P^T ≥0 being the unique positive-semidefinite solution of the algebraic Riccati equation,

$$A^T\mathrm{P} + \mathrm{PA} - w^{-1}PBB^T P = -Q$$

$$\begin{bmatrix} a & b \\ c & d \end{bmatrix}^T \mathrm{P} + \mathrm{P}\begin{bmatrix} a & b \\ c & d \end{bmatrix} - w^{-1}\mathrm{p}\begin{bmatrix} e \\ f \end{bmatrix}[e \quad f]^T\mathrm{P} = -\begin{bmatrix} q_1 & 0 \\ 0 & q_2 \end{bmatrix} \quad (17)$$

The unique positive-semidefinite P can also be expressed as,

$$\mathrm{P} = \begin{bmatrix} \varepsilon & \phi \\ \psi & \epsilon \end{bmatrix}$$

Finally, the output of the vehicle model and the state observer was compared to form a close loop system. In general, there is no other method to direct measure the output of side slip angle. However, yaw rotational speed of a vehicle can be calculated with gyro sensors. In this system, the estimated yaw rotational speed output of state observer unit and the measured yaw rotational speed output of the vehicle model are compared and multiplied by high gain *H*. Then, this gain is fed back into the linear model. The linearized differential equation of eq. (13) becomes

$$\dot{\hat{\mathrm{x}}} = \mathrm{Ax} + \mathrm{BU}_r + \mathrm{CU}_f + H\tilde{r}$$

$$\tilde{r} = \gamma - \gamma^* = \mathbb{C}_2{}^T\hat{\mathrm{x}} - \mathbb{C}_2{}^T\mathrm{x}$$

$$= \mathbb{C}_2{}^T(\hat{\mathrm{x}} - \mathrm{x}) \quad (18)$$

The renewed state observer control input can also be redefined as follow;

$$\mathrm{U}_r = -\frac{1}{r}B^T P(\hat{\mathrm{x}} - \mathrm{x}) + \theta_R \quad (19)$$

9. Simulation Procedure

9.1 Establish a Vehicle Model with OS Characteristic

In the previous section, we mentioned that the vehicle model used the Toyota COMS specification and modified it to represent an OS in-wheel small electric vehicle in the simulation. A simulation of a steady state cornering at various velocity with regard to a constant front steer angle was executed to determine the stability limit velocity of the two wheel steering (2WS) vehicle model. The constant front steer angle is fix at 10° at t=10s. When the yaw rotational speed and the side-slip angle give an infinite value, the velocity is acknowledged as the stability limit velocity.

9.2 Integrating 4WDIS onto the Vehicle Model

A 4WDIS for OS in-wheel small EV was constructed as shown is previous simulation block diagram. In order to investigate the performance of 4WDIS in depth, we have divided the simulation into as follow,

1) Steady state cornering below stability limit velocity and,
2) Steady state cornering over stability limit velocity.

Similar to previous simulation condition, a steady state cornering of a 4WDIS in-wheel small EV at below stability limit velocity and over stability limit velocity, with regard to a constant front steer angle, were carried out. The constant front steer angle is fix at 10° at t=10s. The results of the steady state yaw rotational speed and steady state side-slip angle for 4WDIS are compared to the previous 2WS.

10. Results and Discussions

10.1 Vehicle Model with OS Characteristic

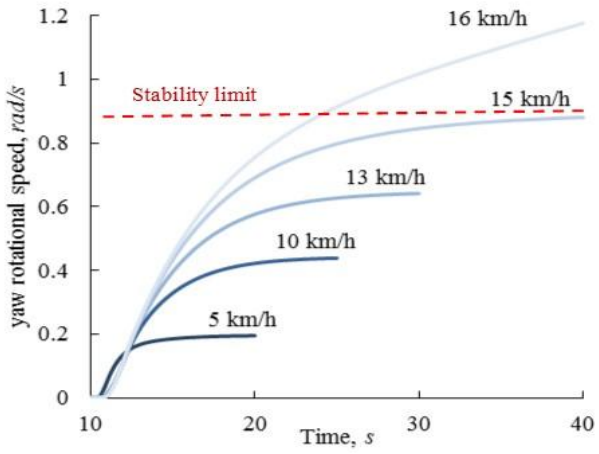

Fig.7 Steady state yaw rotational speed to velocity

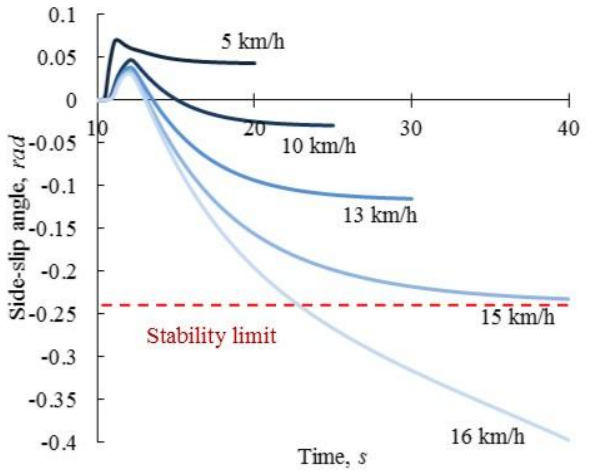

Fig.8 Steady stateside-slip angle to velocity

A simulation of steady state cornering was carried out to determine the stability limit velocity of the OS vehicle model. Fig.(7) and fig.(8) show the results of the steady state yaw rotational speed and steady state side-slip angle in regards to constant front wheel steer angle, respectively. Based on both of these graphs, in regards to constant front steer angle of 10°, the stability limit velocity *Vc* is 15km/h. At this velocity, the vehicle is stable and can reach the maximum steady state yaw rotational speed of 0.90 rad/s with a maximum absolute magnitude of the steady state side-slip angle of 0.24 rad. When the velocity is above 15km/h, the yaw rotational speed and the side-slip angle will give an infinite value. However, the vehicle can still be drive but it is very unstable. Nonetheless, we believe that even in the stable region which is below the stability limit velocity, the OS small EV can be improved. In fig.7, when the constant velocity increased, the longer time it took for the vehicle model to generate a constant yaw rotational speed. This is due to the increase side-slip angle to the constant velocity.

10.2 Steady State Cornering over Stability Limit Velocity with 4WDIS

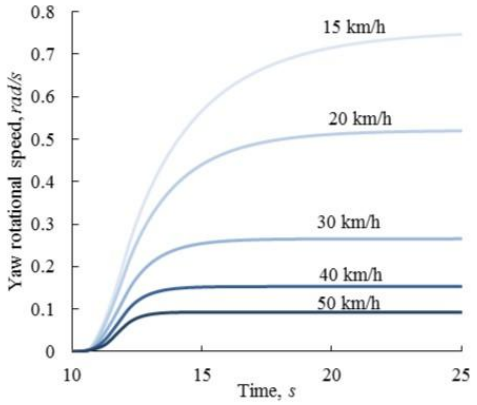

Fig.9 Steady state yaw rotational speed to time change for the vehicle model with 4WDIS

The stability limit velocity of the modelled OS in-wheel small EV has been determined in the previous simulation. The next step is to implement the 4WDIS, which is controlled by the ISCS. The previous steady state cornering simulation condition is repeated again for this vehicle model. In order to have a deep understanding, the discussion is separated between the stability regions.

In this first section, the control effect of the 4WDIS on an OS in-wheel small EV during steady state cornering over the stability limit velocity in regards to constant front steer angle 10° is investigated. Fig.9 shows the result of the steady state yaw rotational speed for the vehicle model with 4WDIS. From this figure, the yaw rotational speed decreased as the velocity of the vehicle model increased. However, if we observe closely, the time to produce a constant steady state yaw rotational speed is instantaneous, especially at velocity range of 30 to 50 km/h. The results of steady state side-slip angle for this simulation in fig.10 shows a reverse pattern from the yaw rotational speed. The side-slip angle increased as the velocity of the vehicle model increased. Based on these results, we can assumed that the 4WDIS control input suppressed the output of yaw rotational speed and side slip angle considerably as the velocity of the vehicle model increased.

In order to understand the control method of the 4WDIS by the ISCS, we have to examine the input of the system. Fig.11 shows the rear wheel steering angle during the steady state cornering simulation of the 4WDIS vehicle model. In the first few second after the front wheel steering angle initiated, the ISCS produced a rear wheel steering angle in minus value that gave the instantaneous yaw rotational speed mention before. The minus angle of the rear wheel was smaller as the steady state velocity increased because the excess yaw rotational speed produce by OS vehicle model also increased. As time progressed, the ISCS gradually increased the rear wheel steering angle to counter the excess yaw rotational speed and maintain a constant value. The angle of the rear wheel is larger at the velocity range over 15 km/h which proofs our early assumption was correct.

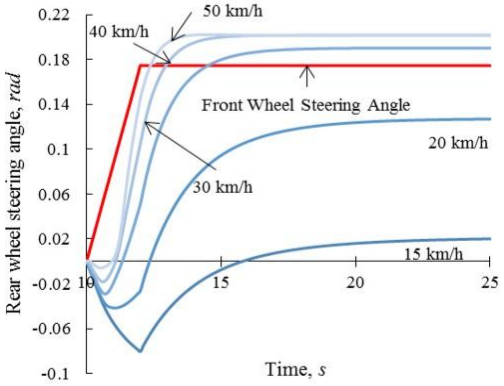

Fig.11 The rear wheel steering angle during the steady state cornering at over stability limit velocity for the vehicle model with 4WDIS

Based on these results, an OS in-wheel small EV can achieve a stable steady state cornering even when the velocity is over the stability limit velocity with the implementation of 4WDIS.

10.3 Steady State Cornering below Stability Limit Velocity with 4WDIS

Theoretically, OS vehicles can already produce high yaw rotational speed and stability when cornering below the stability limit velocity. Logically, any control system is unnecessary in the stable region. Based on the previous result of 2WS, we can assume that the cornering performance in the stable region of the OS in-wheel small EV will be suppressed in the presents of the 4WDIS.

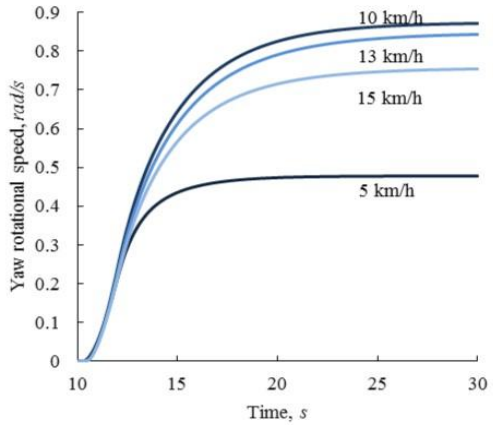

Fig.12 Steady state yaw rotational speed to time change for the vehicle model with 4WDIS

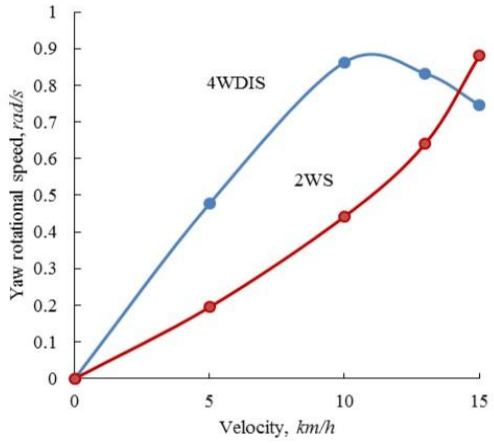

Fig.14 Steady state yaw rotational speed to velocity for the vehicle model with 4WDIS

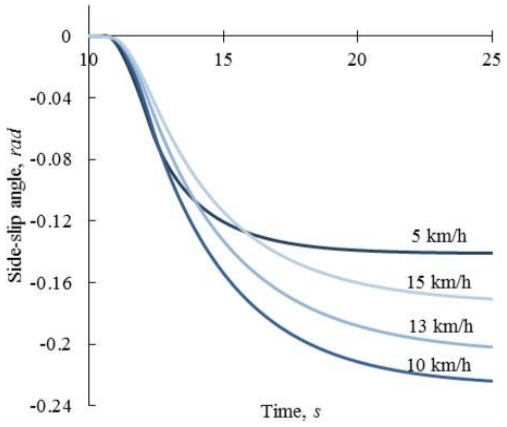

Fig.13 Steady state yaw rotational speed to velocity for the vehicle model with 4WDIS and 2WS

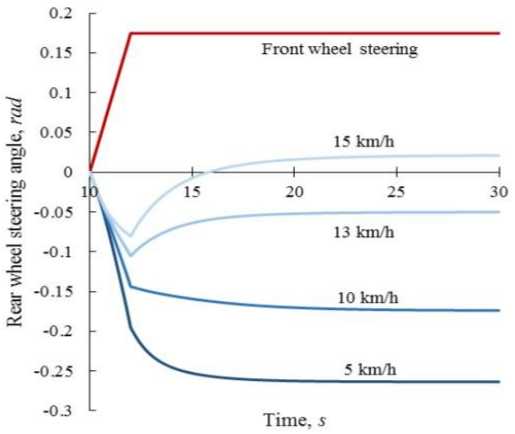

Fig.16 The rear wheel steering angle during the steady state cornering at below stability limit velocity for the vehicle model with 4WDIS

In this section, the control effect of 4WDIS implementation onto an OS in-wheel small EV during steady state cornering below the stability limit velocity in regards to constant front steer angle 10° is presented. Fig.12 and fig.13 show the results of the steady state yaw rotational speed and steady state side-slip angle for the vehicle model with 4WDIS, respectively. The average time for the yaw rotational speed to reach constant value was also reduced to 25s in comparison to the 2WS vehicle model. The 4WDIS had increased the steering response time in regards to the front wheel steer input initiated at t=10s. Even with high yaw rotational speed, the steady state side slip angle also remains constant.

For better comparison, the relation between steady state yaw rotational speed and steady state side-slip angle to the velocity of the vehicle model with 4WDIS and 2WS were plotted in fig.14 and fig.15. The steady state yaw rotational speed of the vehicle model with 4WDIS was approximately two folds the value of vehicle model with normal 2WS at velocity of 0 to 10 km/h. When the velocity of the vehicle increased from 10 km/h to 15 km/h, the steady state yaw rotational speed gradually decreased. A similar pattern occurred for the side-slip angle when we observe in absolute magnitude value.

In order to comprehend these matters, we have to examine the input of the ISCS. Fig.16 shows the rear wheel steering angle during the steady state cornering of the 4WDIS vehicle model. As soon as the front wheel steer initiated at t=10s, the rear wheel steer at the opposite direction as the front wheel. Unlike the situation in the unstable region, the rear wheel steering angle maintained an opposite angle as the front wheel which boost the yaw rotational speed. As the velocity approach near the stability limit, the outputs need to be suppressed.

Conclusion

There are plenty of methods to design an OS vehicle. In this paper, we chose the transfer of weight distribution method to model an OS in-wheel small EV. There are also a few ways to recognize an OS vehicle and one of it is that the vehicle will have a stability limit velocity. When a steady state cornering simulation was carried out below the stability limit velocity *Vc*, the OS in-wheel small EV can achieve steady state cornering with a higher yaw

rotational speed with regards to constant low steering input. However, the moment when velocity $V \geq Vc$, the yaw rotational speed and the side-slip angle produced an infinite value in regards to the same constant steer angle.
The main objective of implementing 4WDIS onto an OS in-wheel small EV is to ensure stability during cornering at any velocity. As a conclusion of to the ISCS control, fig.17 (a) and (b) are the yaw rotational speed and side slip angle characteristics of an in-wheel small EV integrated with our modelled 4WDIS control in comparison to the conventional 2WS vehicle. These figures are a combination from the simulation results of the 4WDIS control simulation.

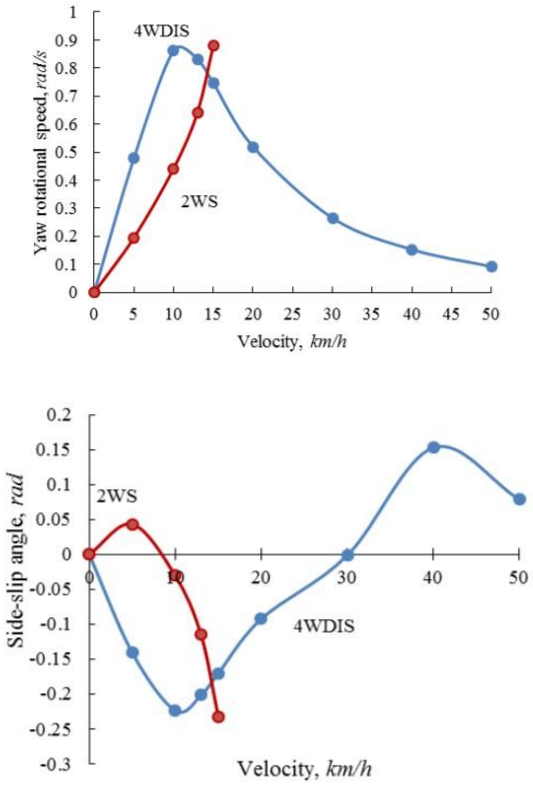

Fig.17 (a) (Upper) Steady state yaw rotational speed to velocity for the vehicle model with 4WDIS
(b) (Lower) Steady state side-slip angle to velocity for the vehicle model with 4WDIS

In this paper, the Intelligence Steering Control System (ISCS) evaluated the dynamic of the in-wheel small EV and dry road surface. In the future, other parameters such as lateral disturbance or icy road surface which has effect on the driving or the vehicle will be taken into simulation analysis.

Lastly, the 4WDIS eliminates the stability limit and ensure a steady state cornering at any velocity.

At the same time, the cornering performance below the stability limit velocity of the OS vehicle can be sustained and improved with the implementation of 4WDIS control

References

[1]. Ministry of Land, Infrastructure and Transport Department of Municipal Affairs and automobile station, Towards the realization of a new social life through the development and utilization of new (mobility) guidelines for the introduction of ultra-small mobility, http: //www.mlit.go.jp / common / 000212867.pdf, June 24, 2010.

[2]. Yoichi Hori, Future Vehicle Driven by Electricity and Control (Research on Four Wheel Motored UOT Electric March II), AMC'02 7th International Workshop on Advanced Motion Control, Maribor, Slovenia.

[3]. Izhar, M., Ogino, H., & Oshinoya, Y. (2013). Research on MOtion COntrol of 4 Wheels Steering Vehicles - Effect of Regeneraive Brake on Vehicle's Motion-. *Proceeding of The School of Engineering, Tokai University*, *53*(2), 99–103.

[4]. Izhar, M., Ogino, H., & Oshinoya, Y. (2014). Research on 4 wheels Independent Steering for Small Electric Vehicle (Effect of Stability Clearance Speed). *Japan Society of Mechanical Engineers 2014 Annual Yearly Conference*,

[5]. Ogino, H., Izhar, M., & Oshinoya, Y. (2012). Stability Analysis of Small Electric vehicle (Effect of Hysteresis of Friction Brake Force for Regenerative Braking Force). *Proceeding of The School of Engineering, Tokai University*, *52*, 55–64.

[6]. Bundorf, R., The Influence of Vehicle Design Parameters on Characteristic Speed and Understeer, SAE Technical Paper 670078, 1967, doi:10.4271/670078.

[7]. Abe, M. (2009). Vehicle Handling Dynamics: Theory and Application. In *Vehicle Handling Dynamics: Theory and Application* (First Edit, p. 352). Butterworth-Heinemann. http://doi.org/10.1016/B978-1-85617-749-8.00002-7

[8]. Ona, E., et al., Clarification and Achievement of Theoratical Limitation in Vehicle Dynamics Integrated Management, journal of Environment and Engineering, Vol. 4, No. 1 (2009), pp.89-100

[9]. Du, F., Li, J. S., Li, L., & Si, D. H. (2010). Robust control study for four-wheel active steering vehicle. *Proceedings - International Conference on Electrical and Control Engineering, ICECE 2010*, 1830–1833. http://doi.org/ 10.1109/iCECE.2010.450

[10]. Hamzah, N., Aripin, M. K., Sam, Y. M., Selamat, H., & Ismail, M. F. (2012). Yaw stability improvement for four-wheel active steering vehicle using sliding mode control. *2012 IEEE 8th International Colloquium on Signal Processing and Its Applications*, 127–132. http:// doi.org/10.1109/ CSPA.2012.6194704

[11]. Tian, J., Chen, N., Yang, J., & Wang, L. (2014). Fractional order sliding model control of active four-wheel steering vehicles. In *ICFDA'14 International Conference on Fractional Differentiation and Its Applications 2014*. http://doi.org/10.1109/ICFDA.2014.6967445

[12]. Ssu-Hsin Yu, John J.Moskwa, A Global Approach to Vehicle Control: Coordination of Four Wheel Steering and Wheel Torques, Journal of Dynamic Systems, Measurement, and Control (1994), Vol.116, pp.659-667